# TOKAMAK FORMATION VIA LOCALIZED HELICITY INJECTION USING TANGENTIAL BOUNDARY FLOWS

P.L. GARCIA-MARTINEZ, R. FARENGO, H.E. FERRARI
CONICET-CNEA & Instituto Balseiro, Centro Atomico Bariloche
San Carlos de Bariloche, RN, Argentina
Email: pablogm@cab.cnea.gov.ar

**Abstract**

.

## 1. INTRODUCTION

Non-solenoidal plasma initiation is a crucial component of many present experiments, as well as future burning plasma devices. This can be achieved through methods such as helicity injection, radiofrequency (RF) waves, or induction from poloidal field (PF) coils [1]. Among helicity injection techniques, localized helicity injection (LHI) employs high-power electron current injectors near the plasma edge to produce thin current filaments that wrap around the plasma in a helical structure. At low injector currents, these filaments follow the nearly unperturbed vacuum magnetic field. As the injected current increases, the configuration becomes unstable and relaxes to a tokamak-like state [2]. Previous experiments have demonstrated the feasibility of this mechanism to form and sustain tokamak plasmas with conventional aspect ratios [3].

The underlying physics of this process is described by the theoretical framework of magnetic relaxation. In its basic form, this principle states that an unstable, turbulent plasma will evolve towards a minimum energy state while conserving its global magnetic helicity [4]. However, this constrained minimization analysis cannot be directly applied to the present situation, where the process is intrinsically dynamic, with helicity being continuously injected and dissipated. The dynamics of magnetic relaxation in complex geometries can be studied using magnetohydrodynamic (MHD) simulations, though this is challenging due to the inherently time-dependent and three-dimensional nature of the problem.

Previous work has used MHD simulations to study flux-rope evolution during the initiation of spherical tokamaks [5]. A key limitation of the standard MHD model is that it does not include charge separation; consequently, an electric potential difference across magnetic field lines can not be modeled. To overcome this, the effect of the injector in such framework was represented as a localized volumetric current source [5].

In this work, we present time-dependent, three-dimensional MHD simulations of the formation and sustainment of tokamak-like plasmas via LHI. Our study has two key differences from previous works. First, we consider the geometry of the TCABR upgrade, a conventional aspect-ratio tokamak [6]. A primary motivation for this effort is to contribute to the design of a solenoid-free startup system for this device. Second, our model implements the helicity injection mechanism through boundary flows, a genuine boundary condition that has been used previously to study relaxation dynamics [7]. Our results demonstrate the feasibility of using LHI to initiate a tokamak-like configuration in the TCABR upgrade geometry. They also indicate that an adequate balance between the helicity injection rate and the vertical magnetic field strength is essential to maximize toroidal current driving.

## 2. MODEL DESCRIPTION

### 2.1. Governing equations and numerical method

Simulations in this study are performed with VAC (Versatile Advection Code) [8], a numerical code originally developed for the astrophysics community, in which the finite-volume method for solving the compressible hydrodynamic and MHD equations is implemented. In particular, this code can be used to solve the isothermal resistive MHD model, which is the one employed in this work. The isothermal-MHD equations are non-dimensionalized using a length scale $L$, a density scale $\rho_0$ and a magnetic field scale $B_0$. With these quantities we can define the Alfvèn velocity scale $c_A = B_0/\sqrt{\mu_0 \rho_0}$, the Alfvèn time $\tau_A = L/c_A$, and the current scale $J_0 = B_0/L\mu_0$.

The resulting dimensionless equations are

$$\frac{\partial \rho}{\partial t} + \nabla \cdot (\rho \mathbf{u}) \quad = \quad 0 \tag{1}$$

$$\frac{\partial \mathbf{u}}{\partial t} + \mathbf{u}\cdot\nabla\mathbf{u} + \beta\frac{\nabla p}{\rho} = \frac{\mathbf{J}\times\mathbf{B}}{\rho} + \tilde{\nu}\nabla\cdot\Pi \quad (2)$$

$$\frac{\partial \mathbf{B}}{\partial t} + \nabla\times\mathbf{E} = 0, \quad (3)$$

where, $\mathbf{J} = \nabla\times\mathbf{B}$, $\mathbf{E} = -\mathbf{u}\times\mathbf{B} + \tilde{\eta}\mathbf{J}$, $\Pi = (\nabla\mathbf{u} + \nabla\mathbf{u}^{\mathrm{T}}) - \frac{2}{3}(\nabla\cdot\mathbf{u})$, $p = c_s^2\rho$ (isothermal assumption), where $c_s$ is the sound speed, and $\beta = \mu_0 p_0/B_0^2 = c_s^2/c_A^2$. The parameter $\tilde{\nu} = \nu/(Lc_A)$ is the dimensionless kinematic viscosity and $\tilde{\eta} = \eta/(\mu_0 L c_A)$ is the dimensionless resistivity, both considered spatially uniform. In this work we use $\beta = 0$ (uniform density), $P_m = \tilde{\nu}/\tilde{\eta} = 1$ (magnetic Prandtl) and $\tilde{\eta} = 10^{-4}$. For simplicity, the length scale is $L = 1$ m and $B_0 = 1$ T (toroidal field at the geometric axis), thus, non-dimensional lengths and magnetic fields coincide numerically with SI units. Time is expressed in Alfvèn times, which gives $t_A \approx 0.2$ $\mu$s, for deuterium at a number density $\sim 10^{-19}$ m$^{-3}$.

### 2.2. Geometry, boundary conditions and run parameters

To model TCABR we consider a toroidal flux conserver with rectangular cross section as the domain for the calculation. The major and minor radii are $R_0 = 0.628$ m and $a = 0.172$ m respectively and the elongation $\kappa$ is 1.45, as indicated in Fig. 1 (a). The boundary conditions for the magnetic field in the flux conserving walls are $(i)$ imposed normal field $\mathbf{B}\cdot\mathbf{n}$ and $(ii)$ zero order extrapolation of tangential field $\nabla(\mathbf{B}\times\mathbf{n})\cdot\mathbf{n} = 0$. In the lateral walls the normal (i.e. radial) field is zero. In the bottom and top ends, the imposed normal field ($B_z$) has the profile shown in Fig. 1 (b). The maximum value $B_{z0}$ of the vertical magnetization is located at the inner limit ($R = R_0 - a$) and has negative values in the band $0.525 < R < 0.625$, for helicity injection purposes as explained below.

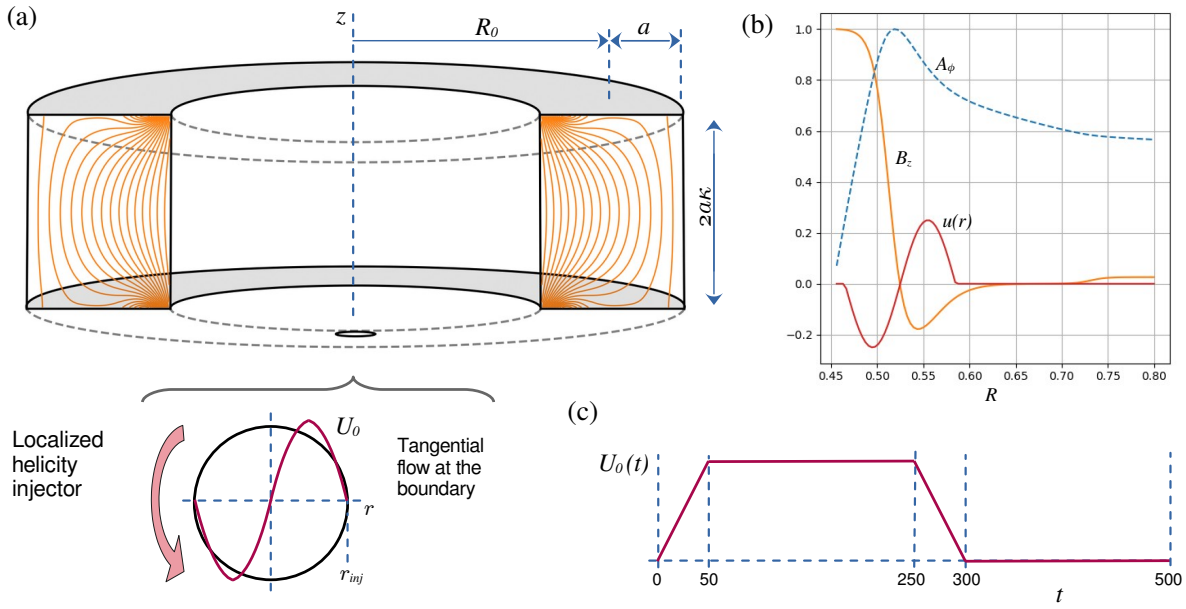


*FIG. 1. (a) (a) Geometry of the flux conserver, vertical magnetization (initial magnetic flux contours in orange) and detail of the localized boundary flow imposed at the bottom end. (b) Profiles of the quantities involved in helicity injection. (c) Time dependence of the amplitude of the imposed driving flow at the boundary.*

The boundary condition for the normal velocity is zero everywhere. Tangential velocity is zero everywhere excepting at the injector, which is modeled as a disc with radius $r_{inj} = 0.06$ in the base, centered at $R_{inj} = 0.525$ and toroidal position $\phi = 0$, as indicated in Fig. 1. Within this disc the tangential velocity is a rotation with sinusoidal profile $u(r)$, where $r$ is the distance to the center of the disc and $u$ points in the azimuthal direction within the disc.

The governing equations are solved in a regular grid with $(55 \times 65 \times 75)$ volumes in cylindrical coordinates $(R, \phi, z)$ during 500 Alfvèn times. The initial condition is the vacuum magnetic field given by the vertical magnetization $B_z$ described before, plus the toroidal field $B_0 R_0/R$ produced by the central solenoid, and zero velocity everywhere. Three runs are analyzed in Sec. 3 with the same tangential flow amplitude $U_0 = 8$ and three different levels of vertical magnetization: $(I)$ $B_{z0} = 0.019$, $(II)$ $B_{z0} = 0.031$ and $(III)$ $B_{z0} = 0.032$, where $B_{z0}$ is the

maximum value of the magnetic field imposed at bottom and top ends of the chamber. Taking $B_{z0}$ as representative of the vertical field and $B_0 = 1$ for the toroidal direction, these values produce field lines that approximately complete $6.5$, $4$ and $2$ toroidal turns during the vertical transit. These values of the characteristic helical ratio $H$ is only indicative, as the vacuum fields vary in $R$ and $z$ and are strongly distorted during intense MHD activity.

### 2.3. Helicity injection

Helicity is given by $K = \int_V \mathbf{A} \cdot \mathbf{B} \, \mathrm{d}^3x$, where $\mathbf{A}$ is the magnetic vector potential. The evolution of helicity is given by [9],

$$\frac{\mathrm{d}K}{\mathrm{d}t} = -2 \int_V \eta \mathbf{J} \cdot \mathbf{B} \, \mathrm{d}V - 2 \int_S \Phi \mathbf{B} \cdot \mathbf{n} \, \mathrm{d}S - 2 \int_S [(\mathbf{A} \cdot \mathbf{B})(\mathbf{u} \cdot \mathbf{n}) - (\mathbf{A} \cdot \mathbf{u})(\mathbf{B} \cdot \mathbf{n})] \, \mathrm{d}S, \tag{4}$$

where the first term describes the resistive dissipation of helicity, the second gives the "dc" helicity injection produced by an applied electrostatic potential $\Phi$ (zero in the MHD framework), the third term involves flow across the boundary (also zero in our case) and finally, the term $(\mathbf{A} \cdot \mathbf{u})(\mathbf{B} \cdot \mathbf{n})$ gives the helicity injection produced by motions of the footpoints of the penetrating magnetic field. This is the relevant term which quantifies the helicity injected by the boundary condition imposed. From the profiles shown in Fig. 1 (b), it is clear that this term in non-zero, in fact, it is negative for positive $U_0$ (for the adopted direction). Note that the center of the disc was intentionally put in the zero crossing of $B_z$, so the two relevant terms, $\mathbf{A} \cdot \mathbf{u}$ and $\mathbf{B} \cdot \mathbf{n}$, simultaneously change their sign.

Relaxed states, i.e. minimum energy states for a given amount of helicity, have uniform $\lambda$ defined as

$$\lambda = \frac{\mathbf{J} \cdot \mathbf{B}}{B^2}. \tag{5}$$

In a driven configurations like the ones considered here, fully relaxed states are never attained. However, relaxation acts to redistribute the current and to flatten the $\lambda$ gradient imposed by the helicity injector. Therefore, the spatial distribution of $\lambda$ is a good indicator whether the configuration is close to a relaxed state (weak driving) or the current profile is dominated by the external driving (see Fig. 4 and the discussion therein for an example).

## 3. RESULTS

### 3.1. Current at the injector and toroidal current

By imposing a localized rotation at the point where the magnetic flux changes sign at the boundary currents must be produced by the twisting of field lines. The value of the net current through the injector driven by this boundary condition can be calculated by integrating $J_z$ in the vicinity of the disc. In practice we integrated $J_z$ throughout all the base. The resulting vertical current is plotted in Fig. 2 (a) for the three runs. As expected from the geometry of the boundary condition and Eq. 4 the net value is negative during the driving phase ($50 < t < 250$), but the sign was inverted in the plot for presentation purposes.

The distribution of $J_z$ at the base in run $(II)$ is shown at two times in Fig. 3 (a) and (b). The current is mainly localized around the injector disc, but there is a significant fraction that flows aligned with the vertical field at other toroidal positions. Several complex structures of pairs of co and counter current channels are formed. These structures have a very rapid dynamics, which explains the level of fluctuations observed in the total vertical current shown in Fig. 2 (a). The distribution of $J_z$ through the top of the chamber is also highly dynamical but is not localized as can be observed in Fig. 3 (c). The difference between the total vertical current through the top and bottom ends is typically below $9\%$.

The currents driven through the base flow along the field lines inducing a toroidal component. This process is approximately linear at the beginning ($t < 50$), as shown in Fig. 2 (b), until a relaxation event produces a significant toroidal current amplification. The current amplification level of this initial relaxation event is proportional to the helicity injection rate, which scales as the square of $B_{z0}$ as can be deduced from the last term in eq. 4. However, the stronger the relaxation event the higher the dissipation which explains the low saturation level con case $(III)$. Note that current after relaxation ($t \approx 80$) for case $(II)$ is twice the current achieved in case $(I)$, which is roughly the same ratio that the helicity injaction rate between these cases. But case $(III)$ relaxes towards a toroidal current $\approx 200$, only a fraction larger than case $(II)$, which has four times less helicity injection rate. Moreover, during sustainment, there is a significant build up of additional toroidal current in cases $(I)$ and $(II)$, as a consequence of smaller intermittent relaxation events, but only a marginal increase in case $(III)$.

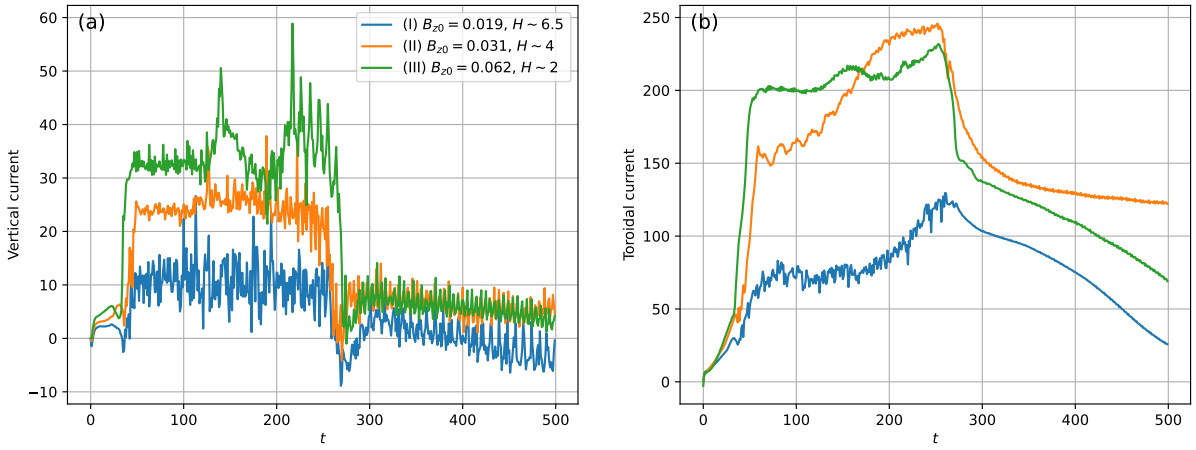


*FIG. 2. Evolution of (a) the vertical current at the base (proxy for the injector current) and (b) the total toroidal current along the plasma for three different magnetization intensities. $H$ is the helical ratio of a typical field line (toroidal turns during the vertical transit).*

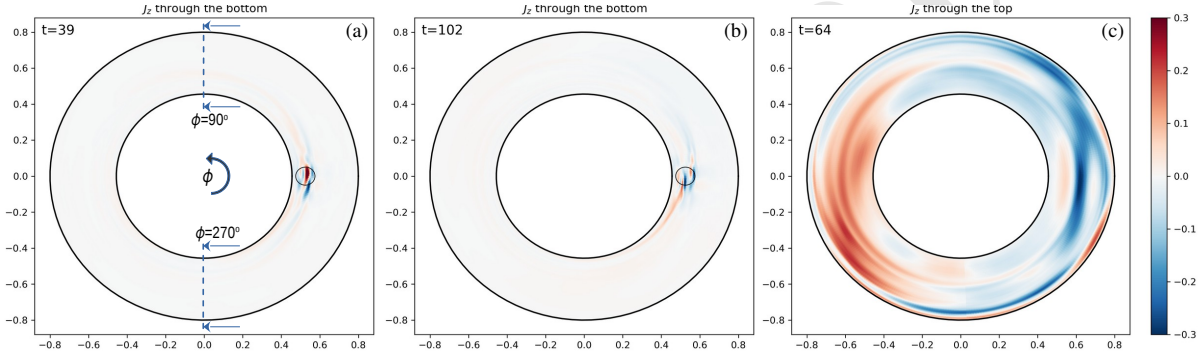


*FIG. 3. Vertical current density distribution at (a-b) the base and at (c) the top for run $(II)$ at different times. The injector disc is indicated with a circle at $\phi = 0$. Panel (a) shows the poloidal planes taken for figures 4, 5 and 6.*

### 3.2. Plasma initiation and sustainment phase

The relaxation event that suddenly increases the toroidal current also involves the formation of closed poloidal flux contours, as shown in Fig. 4 (a) and (d) for cases $(I)$ and $(III)$. These closed contours in $\psi$, the poloidal magnetic flux, result from the integration of $B_z$ in the whole toroidal direction, so they represent an axisymmetric "tokamak-like" structure only in an averaged sense. Due to the high level of fluctuations during sustainment, these contours do not coincide with actual flux surfaces. The contour $\psi = 0$ divides open and closed contours. Closed contours have negative values indicating that toroidal current flows in the negative $\phi$ direction (anti parallel with respect to $B_0$).

Fig. 4 also displays colormaps of $\lambda$, taken at the two specific toroidal positions shown in Fig. 3 (a). Thus, these maps show the toroidal asymmetry of the fluctuation pattern. The panels on left side (a-c) correspond to case $(I)$ that has the weaker driving. In this case, the closed contour region grows gradually during the sustainment phase until it expands to occupy almost all the cross section. Recall that this case has the lowest magnetization level, so the open flux region can be more easily compressed than in the other cases. During the relatively slow expansion of the plasmoid, relaxation acts to flatten the $\lambda$ profile there. Intense $\lambda$ gradients only persist in the region adjacent to the base, where current filaments from the injector are highly localized.

The panels (d-f) on the right of Fig. 4, shown an example of strongly driven configuration. In this case the plasmoid delimited by the $\psi = 0$ contour grows explosively towards the opposite corner of the poloidal plane, as can be inferred from the comparison of panels (d) and (e) which are separated by only 20 Alfvén times. The current filament settles in the outer-top corner and remains there, forming a diagonal negative current channel as the dominant structure during the sustainment phase. The $\lambda$ distribution is highly inhomogeneous in the closed contour region indicating that the driving overcomes the natural tendency of the plasma to relax.

Case $(II)$ has an intermediate level of helicity injection and shows a mixed behavior. In the first relaxation event,

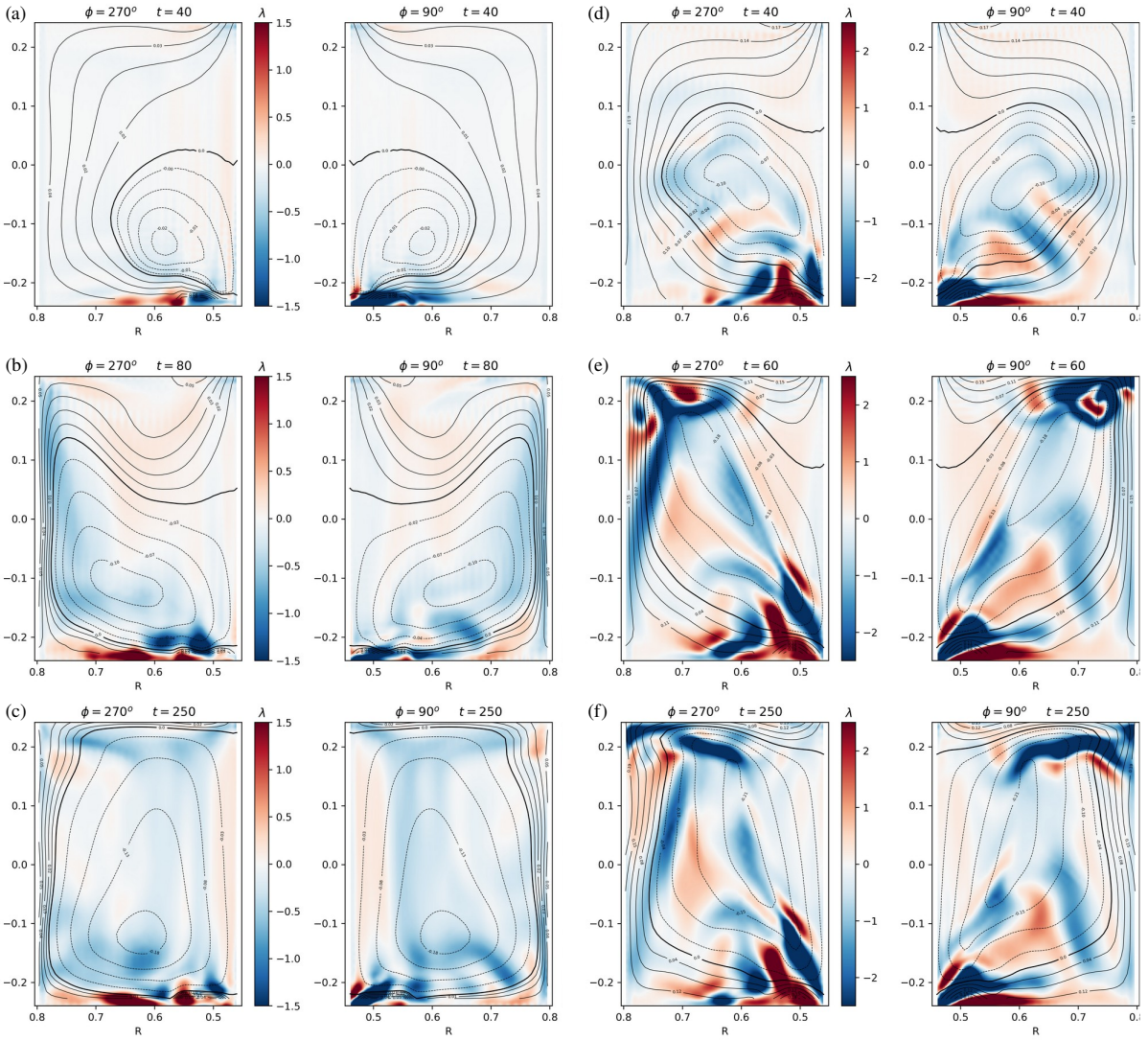


*FIG. 4. Contours of poloidal magnetic flux and colormaps of $\lambda$ in two poloidal planes ($\phi = \pi/2$ and $\phi = 3\pi/2$) at three times for (a-c) case $(I)$ and (d-f) case $(III)$.*

an explosive growth of the plasmoid similar to case $(III)$ is observed, casing the current channel from the injector to concentrate in the outer-top corner of the poloidal plane. However, in this case, a series of smaller relaxation events in the early stage of the sustainment phase (see Fig. 2b at $90 \lesssim t \lesssim 120$) redistribute the current from the injector towards the closed flux region, as can be observed in Fig. 5 (a). As a result, there is a build up of toroidal current during the second half of the sustainment phase, that reaches higher values than the more strongly driven case $(III)$.

### 3.3. Decay phase

When the driving is turned off, in our approach this is done by decreasing $U_0$ to zero in the time interval $250 < t < 300$, the configuration tends to an axisymmetric tokamak state. A large scale fluctuation persists, which nonetheless produces a periodic bouncing of the main negative current channel and the closed flux contours. This fluctuation is observed as a positive flowing current density ($\lambda$ in the plot) in high field side at $\phi = 90°$ in Fig. 6 (a) and at $\phi = 270°$ in Fig. 6 (b). There are also persistent high frequency fluctuations near the bottom and the injector that prevent the vertical current at the base from going exactly to zero (see Fig. 2a).

The behavior of the toroidal current in the decay phase, $t > 300$, observed in Fig. 2 (b) is clarified by the comparison of the configurations at $t = 300$ shown in Fig. 6. Due to the lower helicity injection rate in case $(II)$, relaxation events were able to redistribute more current into the closed contour region, thus, more magnetic flux is trapped there when sustainment ceases. In addition, the magnetization is weaker in this case, so the ratio closed

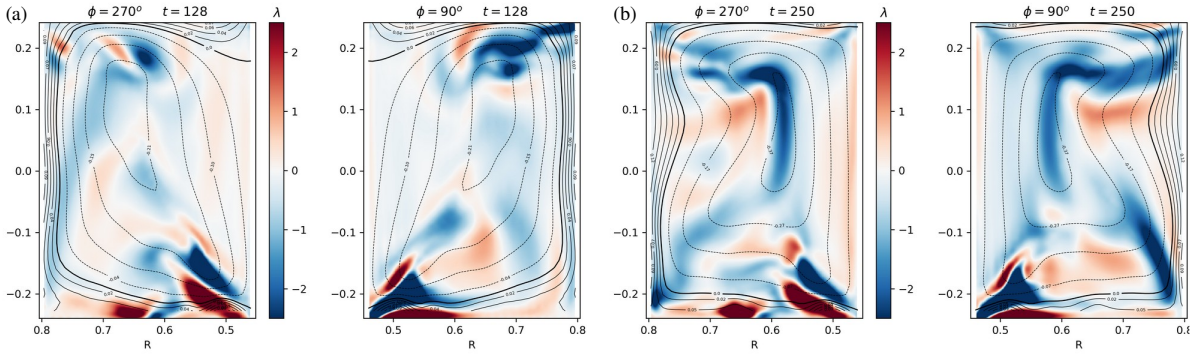


*FIG. 5. Contours of poloidal magnetic flux and colormaps of $\lambda$ in two poloidal planes ($\phi = \pi/2$ and $\phi = 3\pi/2$) at three times for case $(II)$ (a) at $t = 128$ during sustainment and (b) at $t = 250$ when sustainment is gradually turned off.*

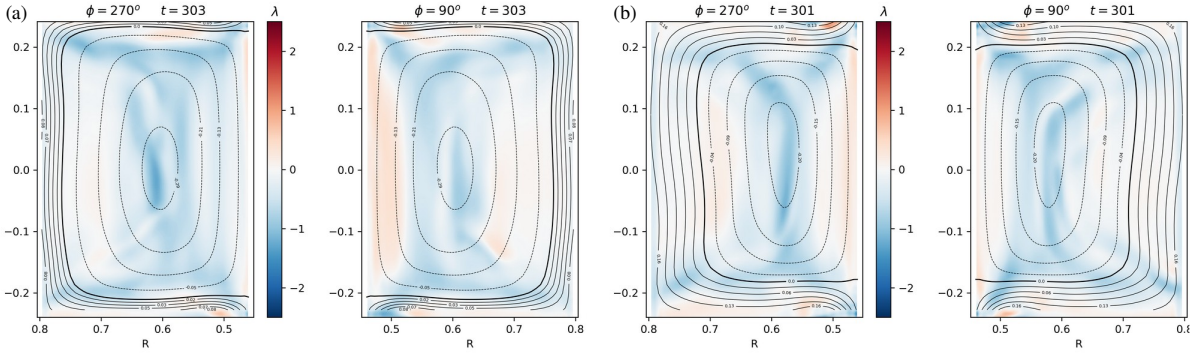


*FIG. 6. Contours of poloidal magnetic flux and colormaps of $\lambda$ in two poloidal planes ($\phi = \pi/2$ and $\phi = 3\pi/2$) during the decay phase for cases (a) $(II)$ and (b) $(III)$.*

to open flux is significantly larger in this case: $\sim 0.3/0.08 \approx 4$ in case $(II)$ compared to $\sim 0.21/0.16 \approx 1.3$ in case $(III)$.

Another interesting aspect of the decay phase is the decay rate of toroidal current (and poloidal flux) just after the sustainment flat-top ($250 < t < 300$). Cases $(II)$ and $(III)$ experience a very rapid drop due to the high current gradients present in strongly driven configurations. Case $(I)$ instead, exhibits only a gentle decay, since the dynamics of relaxation was able to redistribute current at a rate similar to the current injection rate.

## 4. CONCLUSIONS

Time-dependent, three-dimensional magnetohydrodynamic (MHD) simulations have been performed to investigate the formation and sustainment of a tokamak-like plasma via localized helicity injection (LHI) in the geometry of the TCABR upgrade. Helicity injection was produced by tangential boundary flows applied as a small disc at the bottom boundary of the chamber that rotated over a surface encompassing incoming and outgoing penetrating magnetic flux. The simulations successfully capture the formation of closed poloidal flux surfaces following a magnetic relaxation event, transitioning from open vacuum field lines to a confined plasma state. This demonstrates the fundamental feasibility of initiating a tokamak-like configuration in a conventional aspect-ratio tokamak using LHI modeled as a boundary flow condition.

The key findings of this study are as follows:

- Case (I) - Low Bz0: Under weak driving, the system undergoes a gradual relaxation, leading to a well-distributed current profile and a slowly expanding plasmoid. However, the overall achieved toroidal current remains modest.
- Case (III) - High Bz0: With strong driving, an explosive initial relaxation occurs, but the configuration becomes overly dominated by the injector. The current remains concentrated in a filament, preventing efficient current redistribution into the core and leading to high dissipation and a lower saturation current despite a higher injection rate.

- Case (II) - Intermediate Bz0: An optimal regime was identified. Here, the initial relaxation is significant, and subsequent, smaller relaxation events during the sustainment phase effectively redistribute current from the edge injector into the closed flux region. This results in a higher final toroidal current and a larger ratio of closed-to-open magnetic flux, representing the most efficient current drive scenario.

The Role of Helicity Injection and Magnetization Balance: A central conclusion is that the efficacy of the startup is critically dependent on achieving an adequate balance between the helicity injection rate and the vertical magnetic field strength Bz0.

Current Multiplication [10]: The current amplification factor—the ratio of toroidal plasma current to the injector current—was found to be highly sensitive to this balance. The intermediate case (II) achieved the most effective current multiplication, outperforming the more strongly driven case (III). This finding is consistent with experimental observations, such as those from the Pegasus Toroidal Experiment [10], where current amplification factors were also found to be optimal within a specific operational window, rather than increasing monotonically with injector power.

Sustainment and Decay Dynamics: The sustainment phase is characterized by intermittent relaxation activity, which is crucial for continually feeding current into the plasma core. Upon cessation of the driving flow, configurations that experienced more effective relaxation (Cases I and II) transitioned to a decaying, more axisymmetric state with a slower current decay rate, while the strongly driven case (III) exhibited a rapid current drop due to steep, unsustainable current gradients.

In summary, this work provides numerical evidence that LHI via boundary flows is a viable solenoid-free startup method for conventional tokamaks like the TCABR upgrade. The success of this approach hinges not on maximizing the helicity injection rate alone, but on optimizing it relative to the confining vertical field to encourage beneficial relaxation dynamics that enhance the current multiplication factor. Future work will involve more detailed scans of the parameter space and direct quantitative comparisons with experimental data to further refine this startup scenario.

## REFERENCES

[1] RAMAN, R. et al., Solenoid-free plasma startup in spherical tokamaks, Plasma Phys. Control. Fusion **56** 103001 (2014).

[2] BONGARD, M. W. et al., Advancing local helicity injection for non-solenoidal tokamak startup, Nucl. Fusion **59** 076003 (2019).

[3] ONO, M. et al., Steady-state tokamak discharge via dc helicity injection, Phys. Rev. Lett. **59** 2165 (1987).

[4] TAYLOR, J. B., Relaxation and magnetic reconnection in plasmas, Rev. Mod. Phys. **58** 741 (1986).

[5] O'BRYAN, J. et al., Simulated flux-rope evolution during non-inductive startup in Pegasus, Plasma Phys. Control. Fusion **56** 064005 (2014).

[6] BOUZAN, A. S. et al., Structural analysis of the in-Vessel RMP IM-Coils of the TCABR tokamak, IEEE Transactions on Plasma Science **52** n. 9 p. 3847 (2024).

[7] GARCIA-MARTINEZ, P. L. et. al., Spheromak formation and sustainment by tangential boundary flows, Phys. Plasmas **17** 050701 (2010).

[8] TOTH, G., General Code for Modeling MHD flows on Parallel Computers: Versatile Advection Code, Astrophys. Lett. Commun. **34** 245 (1996).

[9] BERGER, M. A., Introduction to magnetic helicity, Plasma Phys. Control. Fusion **41** B167 (1999).

[10] BATTAGLIA, D. J. et al., Tokamak startup using outboard current injection on the Pegasus Toroidal Experiment, Nucl. Fusion **51** 073029 (2011).